Contribution from the Istituto di Chimica Fisica,
Università di Roma, Rome, Italy

Configurational Effect of Iron(III) Complex Ions in the Disproportionation of Hydrogen Peroxide. A Kinetic Investigation as a Function of pH

MARIO BARTERI, MARCELLO FARINELLA, BASILIO PISPISA,* and LUCIANO SPLENDORINI

Received March 10, 1978

The decomposition of hydrogen peroxide catalyzed by configurationally different iron(III) complex ions, i.e., *cis*-Fe(bmen)X_2^{n+} and *trans*-Fe(tetpy)X_2^{n+} (where bmen = *N,N'*-bis(2-methylpyridyl)ethylenediamine, tetpy = 2,2':6',2'';6'',2'''-tetrapyridyl and X = H_2O or OH^-, depending on pH), has been investigated. The order of the Fe(bmen)X_2^{n+}-catalyzed reaction is unity with respect to both H_2O_2 and the metal compound, within the whole range of pH explored (3.5–7.3). In contrast, within the pH range 6–8.5, the reaction carried out on quaterpyridineiron(III) derivative may be described by mixed total second- and third-order kinetics, the higher degree mechanism being predominant at high substrate concentration. At fixed concentration of complex ions, saturation phenomena are observed in all cases on increasing the concentration of H_2O_2. As expected, the Lineweaver–Burk plot of the Fe(bmen)X_2^{n+}-catalyzed reaction is linear whereas it is nonlinear (at high substrate concentration) when the trans complex ions are used. The steady-state rate laws were derived and the calculated reaction velocities were found to agree satisfactorily with those experimentally determined. At 25 °C, the rate constant for the irreversible decomposition of the Michaelis complex, which represents the rate-limiting step, is 3.2 ± 0.2 and 4.8 ± 0.3 s^{-1} for the Fe(bmen)X_2^{n+} and Fe(tetpy)X_2^{n+} ions, respectively. The energy of activation of this step is 10.6 ± 1.6 and 7.5 ± 1.2 kcal/mol and the entropy of activation (298 K) is −23 ± 5 and −32 ± 4 eu, respectively. Implications of the role played by the different topologies of the complex ions in the kinetics of the catalysis as well as in the activation parameters are discussed.

Introduction

The decomposition of hydrogen peroxide has been demonstrated to occur within the coordination sphere of iron(III) complexes.[1-5] The question as to whether the topology of the catalyst influences the kinetics of the process has not yet received, however, a definite answer. Moreover, most of the studies are lacking a detailed investigation on the protolytic state of the intermediate peroxo adduct. This prevents a strict comparison of the results, often obtained at different pH's.

We present the data of a kinetic investigation on the disproportionation of H_2O_2, within a wide range of pH. Configurationally different pseudooctahedral Fe(III) derivatives were used as catalysts, i.e., *cis*-Fe(bmen)X_2^{n+} and *trans*-Fe(tetpy)X_2^{n+} (where bmen = *N,N'*-bis(2-methylpyridyl)-ethylenediamine, tetpy = 2,2':6',2'':6'',2'''-tetrapyridyl, and X = H_2O or OH^-, depending on pH). The aim of the work was, first, to elucidate the role played by the configuration of the complex ions on the kinetics of the process and, second, to investigate the effect of pH on the reaction velocity.

Both of these parameters were found to influence the decomposition of hydrogen peroxide, through the peroxo intermediate. A change in reaction rate is observed within the pH range where the protolysis of the peroxo adduct is expected to occur. On the other hand, evidence of a diverse reaction mechanism is obtained and will be discussed in the light of the different topologies of the complex ions employed.

Experimental Section

Materials. The pseudooctahedral Fe(III) complexes were prepared as already described.[6,7] The cis compound may be formulated as a mononuclear species both in the solid state and in aqueous solution.[6] The *trans*-quaterpyridineiron(III) derivative is an oxo-bridged dimeric compound in the solid state.[7] In solution, at the pH's and concentrations with which we are primarily concerned, it is almost entirely in the mononuclear form.[8] This is also confirmed by the results of kinetic experiments shown later. According to potentiometric titrations, the protolytic equilibrium between the hydroxoaquo and dihydroxo species has a pK_a = 4.2 ± 0.1 and pK_a' = 6.3 ± 0.1 (25 °C) for cis and trans compounds, respectively.

Analytical grade, stabilizer-free H_2O_2 (C. Erba, Milan) was used without further purification. Only very little decomposition occurred in the absence of complex ions. This was taken into account each time by blank experiments. Acetate or Tris buffer, 0.01 mol L^{-1}, was used, but in some cases pH was adjusted by adding appropriate amounts of standard acid or base. Only very small differences were noted for the two methods.

All measurements were performed on freshly prepared solutions, using double-distilled water with a conductivity less than 2×10^{-6} Ω^{-1} cm^{-1} (20 °C).

Methods and Apparatus. Kinetic experiments were carried out as follows. Equal volumes of buffered catalyst and H_2O_2 solutions were kept at constant temperature before mixing. The reaction mixtures had total volumes of 10 mL and were maintained under vigorous stirring and at constant temperature (±0.1 °C). The reaction was stopped at short time intervals by blowing 1.5 mol L^{-1} H_2SO_4 containing 0.05 mol L^{-1} KF into the mixture, and the unreacted substrate was then directly titrated, usually employing standard ceric sulfate and (*o*-phenanthroline)iron(II) as indicator. In a few cases a Warburg-type apparatus was employed and the decomposition of H_2O_2 was followed manometrically. The two methods gave similar results, within experimental errors.

The initial reaction velocity, $V_0 = -d[H_2O_2]/dt$ (mol L^{-1} s^{-1}) was evaluated from the slope of H_2O_2 concentration–time curves at t = 0, the extent of decomposition being generally limited to about 15–20% of the original concentration.

Absorption spectra were determined on a Beckman DK-2A spectrophotometer with appropriate quartz cells. The pH measurements were made with a Radiometer 26 pH meter using semimicroelectrodes.

Results and Discussion

***cis*-Fe(bmen)X_2^{n+}.** At constant initial concentration of both substrate and complex ions, the catalysis of H_2O_2 in dilute solution varies with pH, as shown by the empty symbols in Figure 1a. The initial reaction rate (V_0) is proportional to $1/[H^+]$ at pH <5 whereas it becomes $[H^+]$ independent above this pH.

Typical curves of the dependence of initial reaction velocity on the initial concentration of substrate, at fixed complex concentration and at various pH's, are presented in Figure 2. Within the whole range of pH explored, at low $[H_2O_2]$ the rate of catalysis follows first-order saturation kinetics. E.g.

$$V = V_m[H_2O_2]/([H_2O_2] + K_M) \quad (1)$$

where V_m is the "saturation" velocity and K_M is the Michaelis constant. The Lineweaver–Burk[9] plot of these data ($1/V_0$ against $1/[H_2O_2]_0$) gives, therefore, straight lines, whose intercepts I and tangents T (obtained by the least-squares method using V_0^2 weight factors) for different pH values are

0020-1669/78/1317-3366$01.00/0

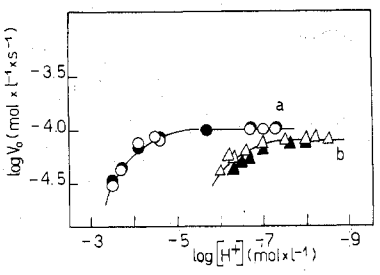

Figure 1. Initial rate of decomposition of hydrogen peroxide as a function of pH, at fixed catalysts and substrate concentration (empty symbols): curve a, *cis*-Fe(bmen)X_2^{n+} complex ions; curve b, *trans*-Fe(tetpy)X_2^{n+} complex ions. $[C]_0 = 1 \times 10^{-4}$ mol L^{-1}, $[H_2O_2]_0 = 4 \times 10^{-2}$ mol L^{-1}, $T = 26$ °C, acetate or Tris buffer (0.01 mol L^{-1}). Full symbols indicate calculated reaction velocities, according to eq 4 (a) and to the reciprocal of eq 7 (b); see text.

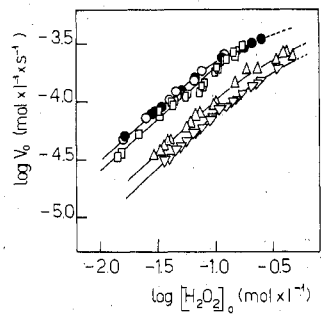

Figure 2. Initial rate of decomposition of H_2O_2 as a function of the initial concentration of substrate, at fixed 1×10^{-4} mol L^{-1} Fe(bmen)X_2^{n+} complex ion concentration, $T = 25$ °C, and pH 3.5 (▽), 3.7 (△), 4.6 (□), 6.7 (○), and 7.3 (●).

Table I. Kinetic Parameters of the Lineweaver–Burk Plot for the Decomposition of H_2O_2 Catalyzed by Fe(bmen)X_2^{n+} Ions (25 °C; $[C]_0 = 1 \times 10^{-4}$ mol L^{-1})

pH	T,[a] s	I,[a] s L mol^{-1}
3.52	1145 ± 61	1977 ± 101
3.67	834 ± 33	1760 ± 76
4.10	555 ± 18	1641 ± 51
4.63	379 ± 18	1544 ± 70
5.68	350 ± 11	1514 ± 47
6.72	323 ± 10	1591 ± 46
7.30	323 ± 10	1591 ± 46

[a] Obtained by the least-squares method.

reported in Table I. The dependence on $[H^+]$ of these parameters may be empirically expressed as

$$I = (1.45 \pm 0.19) \times 10^6[H^+] + (1560 \pm 112)$$
$$T = (2.58 \pm 0.17) \times 10^6[H^+] + (332 \pm 18) \quad (2)$$

On the other hand, according to empirical rate eq 3 at fixed

$$-d[H_2O_2]/dt = k[H_2O_2]^n[C]^m \quad (3)$$

$[C]_0/[H_2O_2]_0 < 1$ ratio, a plot of log V_0 against log $[H_2O_2]_0$ should give a straight line whose slope is the total order of the reaction $(n + m)$.[10] $[C]_0$ and $[H_2O_2]_0$ denote the initial concentration of complex ions and substrate, respectively. This is indeed the case, as shown in Figure 3a, where the slope of the curve is 2. Since the partial order of the reaction with respect to the complex ions is nearly unity (Figure 4a), it may be concluded that the rate-determining step of the catalysis on *cis*-Fe(bmen)X_2^{n+} ions involves one molecule of substrate per molecule of complex.

On the basis of these results, the mechanisms of Scheme I may be taken into account, where L denotes the bmen ligand. This scheme predicts that two molecules of H_2O_2 are decomposed on each cycle.[1,2,5,11] Furthermore, pathway a is $[H^+]$ independent while pathway b depends on pH since the Michaelis complex undergoes a protolytic equilibrium before reacting further. This would explain the observed increase of the initial velocity with decreasing $[H^+]$ (Figure 1a).

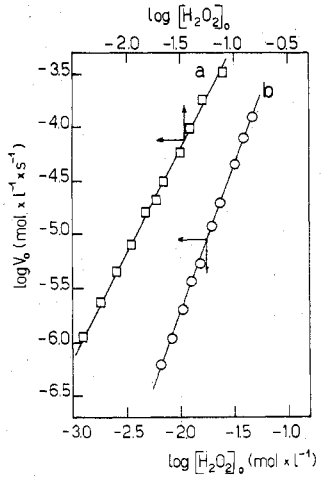

Figure 3. Decomposition of H_2O_2 catalyzed by Fe(bmen)X_2^{n+} (a) and Fe(tetpy)X_2^{n+} (b) ions. Initial reaction velocity as a function of the initial concentration of substrate, at a fixed [complex]/[substrate] molar ratio of 0.0025: curve a, pH 7.0; curve b, 7.6 (Tris buffer 0.01 mol L^{-1}, $T = 26$ °C).

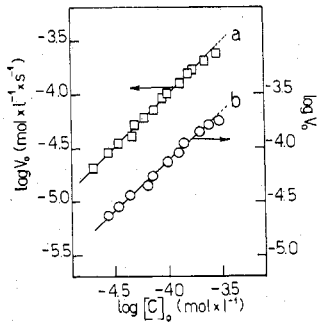

Figure 4. Initial rate of decomposition of H_2O_2 as a function of the initial concentration of complex ions, at a fixed substrate concentration of 4×10^{-2} mol L^{-1}: curve a, cis compound (pH 7.0); curve b, trans compound (pH 7.6) (Tris buffer 0.01 mol L^{-1}, $T = 25$ °C).

Scheme I

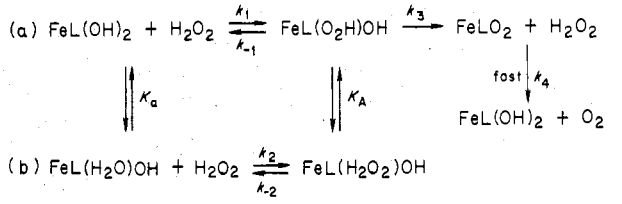

The steady-state rate of decomposition is then given by

$$\frac{-d[H_2O_2]}{dt} = \frac{2k_3[C]_0[H_2O_2]}{[H_2O_2](1 + [H^+]/K_A) + K_M'[H^+]/K_A + K_M''} \quad (4)$$

where $K_M' = (k_{-2} + k_3)/k_2$ and $K_M'' = (k_{-1} + k_3)/k_1 + k_3/k_4$. As a first approximation, k_3/k_4 can be neglected since experiments at very low substrate concentration ($[C]_0/[H_2O_2]_0 \geq 1$) indicate that $k_4 >> k_3$. The intercepts I and tangents T of the Lineweaver–Burk plot have, therefore, the form

$$I = \{([H^+]/K_A) + 1\}/2k_3[C]_0$$
$$T = \{[(k_{-2} + k_3)/k_2][H^+]/K_A + (k_{-1} + k_3)/k_1\}/2k_3[C]_0 \quad (5)$$

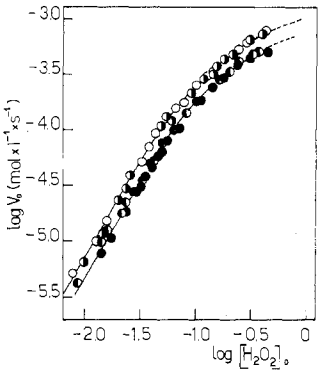

Figure 5. Initial rate of decomposition of H_2O_2 as a function of the initial concentration of substrate, at fixed Fe(tetpy)X_2^{n+} complex ion concentration of 1×10^{-4} mol L^{-1}, $T = 25$ °C, and pH 6.3 (●), 6.7 (◐), 7.6 (◑), and 8.0 (○).

Comparing (5) with the empirical expressions (2), one easily obtains $k_3 = 3.22 \pm 0.23$ s^{-1}, $K_A = (1.25 \pm 0.40) \times 10^{-3}$ mol L^{-1}, $(k_{-2} + k_3)/k_2 = 2.08 \pm 0.42$ mol L^{-1}, and $(k_{-1} + k_3)/k_1 = 0.214 \pm 0.025$ mol L^{-1} (25 °C). When the reaction rate is calculated according to eq 4 using these parameters, the initial reaction velocities (full symbols in Figure 1a) are in very good agreement with those experimentally determined, in the whole range of pH explored. Furthermore, at pH's >5 (e.g., when $[H^+]/K_A << 1$), eq 4 reduces to eq 3 if $[H_2O_2] + K_M'[H^+]/K_A << K_M''$. Under these conditions, the second-order rate constant is $k = 2k_3/K_M''$. At 25 °C and pH 6.7–7.3, k is found to be 30.9 ± 3.5 L mol^{-1} s^{-1} as compared to $k_{obsd} = 28.8$ L mol^{-1} s^{-1} (26 °C, pH 7), which may be graphically evaluated from the data of Figure 3a.[10]

trans-**Fe(tetpy)X_2^{n+}.** The initial reaction rate as a function of pH, at constant initial concentration of both substrate and complex ions, has a trend similar to that previously discussed, but it becomes $[H^+]$ independent only above about pH 7.5 (empty symbols in Figure 1b).

The effect of substrate concentration on the kinetics of the process, at fixed $[C]_0 = 1 \times 10^{-4}$ mol L^{-1}, was investigated over a range of pH. Typical saturation curves are given in Figure 5. This time, however, the slope of the linear portion of the curves is fractional; e.g., the apparent partial order with respect to H_2O_2 is found to be 1.7. This finding cannot be blamed upon a possible systematic error in the experimental method since, under the same conditions, the data taken from *cis*-Fe(bmen)X_2^{n+} ions strictly yield first-order saturation kinetics (Figure 2). In addition, the total order of reaction evaluated from the slope of the straight line in Figure 3b (see above) is 2.8 whereas the partial order of reaction with respect to the complex ions is unity (Figure 4b). It may be concluded, therefore, that the nonlinear behavior of the Lineweaver–Burk plots of Figure 6 arises from a second-order mechanism with respect to the substrate, though, under the experimental conditions used, a parallel first-order pathway very likely occurs to some extent. In the former case the rate-determining step involves the irreversible decomposition of a ternary Michaelis adduct, in which both apical sites of the complex ions are engaged by substrate species, while in the latter it involves the decomposition of a monoperoxo complex.

On the basis of these results, the mechanisms of Scheme II may be considered,[5] where this time L denotes tetpy ligand. The scheme predicts the occurrence of two parallel reactions; e.g., H_2O_2 may decompose either through pathway b via a diperoxy Michealis complex or through the low-$[H_2O_2]$ catalytic pathway a in which only one active site is occupied with the substrate. Reaction a′ should take into account the observed increase of the initial rate with decreasing $[H^+]$ (Figure 1b).

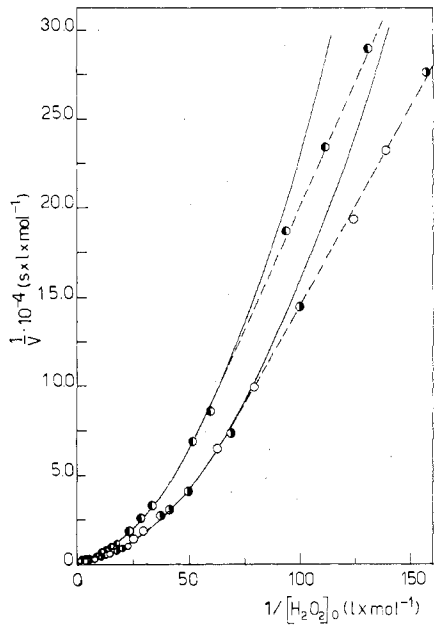

Figure 6. Lineweaver–Burk plot for the Fe(tetpy)X_2^{n+}-catalyzed reaction at pH 6.7 (◐), 7.6 (◑), and 8.0 (○) ($T = 25$ °C, $[C]_0 = 1 \times 10^{-4}$ mol L^{-1}). The solid lines refer to the least-squares best fit to the experimental data for $[H_2O_2]_0 > 2 \times 10^{-2}$ mol L^{-1} (cf. eq 7), using V_0^2 weight factors (see text).

Scheme II

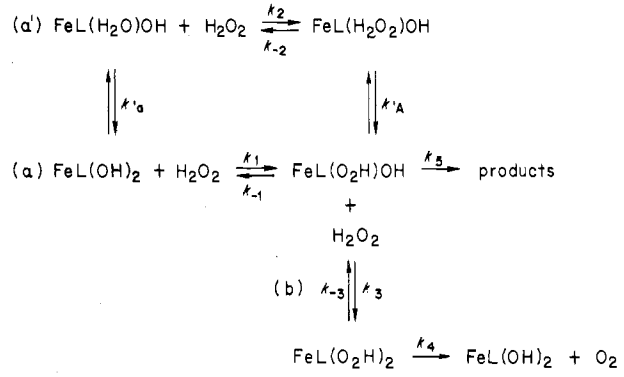

In the steady state, the rate of decomposition is then given as

$$-d[H_2O_2]/dt = \{2k_4[C]_0[S]^2 + 2k_5[C]_0[S]K_M\}/\{[S]^2 + [S](K_M(1 + [H^+]/K_A') + K_M') + K_M(K_M'' + K_M''')\} \quad (6)$$

where $K_M = (k_{-3} + k_4)/k_3$, $K_M' = k_4(k_1 + k_2)/k_1k_2$, $K_M'' = (k_{-2}[H^+]/k_2K_A') + k_5/k_2$, and $K_M''' = (k_{-1} + k_5)/k_1$.

It was found, however, that the mixed third- and second-order mechanisms (Scheme II) provided no method of obtaining mechanistically meaningful constants (such as k_5) from the available data, even under simplifying assumptions (see Appendix). On the other hand, at high substrate concentration the higher degree mechanism definitely predominates. When $[H_2O_2]_0$ is higher than about 2×10^{-2} mol L^{-1}, the Lineweaver–Burk plots obey the parabolic equation $y = I' + T'x + T''x^2$ which describes the pure total third-order reaction according to the foregoing mechanism (see below). Therefore, under these conditions, we may disregard the parallel total second-order kinetics as a first approximation.

The reciprocal form of the steady-state rate of decomposition for the high-$[H_2O_2]$ catalytic pathway is given by

$$\frac{-dt}{d[H_2O_2]} = \frac{1}{2k_4[C]_0} + \frac{K_M(1 + [H^+]/K_A') + K_M'}{2k_4[C]_0}\frac{1}{[H_2O_2]} + \frac{K_M[(K_{-2}[H^+]/k_2K_A') + k_{-1}/k_1]}{2k_4[C]_0}\frac{1}{[H_2O_2]^2} \quad (7)$$

Equation 7, which is reminiscent of that developed for enzymatic processes where a ternary Michaelis complex is formed,[12] predicts a nonlinear behavior when $1/V_0 = y$ is plotted against $1/[H_2O_2]_0 = x$. This is the case above about $[H_2O_2]_0 = 2 \times 10^{-2}$ mol L^{-1}, as shown by the full lines in Figure 6 drawn as the least-squares best fit to the experimental data based upon a regression calculation using V_0^2 weight factors.

The $[H^+]$ dependence of coefficients T' and T'' of the parabolic equation is illustrated in Figure 7. From the results one has

$$y = (1050 \pm 60) + [(3.33 \pm 0.62) \times 10^8[H^+] + (161 \pm 14)]x + [(0.26 \pm 0.05) \times 10^8[H^+] + (13.7 \pm 1.2)]x^2 \quad (8)$$

Comparing eq 7 with the empirical expression (8), one easily obtains $k_4 = 4.8 \pm 0.3$ s^{-1}, $K_M + K_M' = 0.155 \pm 0.023$ mol L^{-1}, $K_M/K_A' = (3.23 \pm 0.60) \times 10^5$, $K_Mk_{-1}/k_1 = (1.32 \pm 0.2) \times 10^{-2}$ mol^2 L^{-2}, and $k_{-2}/k_2 = (8.8 \pm 0.4) \times 10^{-2}$ mol L^{-1} (25 °C).

When the reaction velocities are calculated according to the reciprocal of eq 7 using these parameters, there is a satisfactory agreement with the experimentally determined initial rates only at high substrate concentration. For example, $V_0 = (7.30 \pm 0.46) \times 10^{-5}$ and $(8.16 \pm 0.50) \times 10^{-5}$ mol L^{-1} s^{-1} at pH 7 and 8, respectively, while under the same experimental conditions ($[C]_0 = 1 \times 10^{-4}$, $[H_2O_2]_0 = 4 \times 10^{-2}$ mol L^{-1}, 25 °C), the calculated velocities are $(6.40 \pm 1.40) \times 10^{-5}$ and $(7.38 \pm 1.53) \times 10^{-5}$ mol L^{-1} s^{-1} (full symbols in Figure 1b). In contrast, all things being equal but $[H_2O_2]_0$ (=4×10^{-3} mol L^{-1}), $V_0 = (1.58 \pm 0.12) \times 10^{-6}$ and $(1.73 \pm 0.13) \times 10^{-6}$ mol L^{-1} s^{-1} [13] whereas the calculated velocities are $(8.8 \pm 1.9) \times 10^{-7}$ and $(1.0 \pm 0.2) \times 10^{-6}$ mol L^{-1} s^{-1}, respectively. As expected, in the latter case there is a large discrepancy between the experimental and calculated initial rates, which indicates that the second-order parallel reaction cannot be any more neglected. Further experiments at very low $[H_2O_2]_0$ are needed to discriminate quantitatively the kinetic contribution of each pathway.

True Activation Energy. The Arrhenius plot for the irreversible decomposition of the Michaelis adduct in the pH region where the reaction catalyzed by both complex ions is practically $[H^+]$ independent is illustrated in Figure 8. According to these data, the true activation energy of the process is 10.6 ± 1.6 and 7.5 ± 1.2 kcal/mol for *cis*-Fe(bmen)$X_2]^{n+}$ and *trans*-Fe(tetpy)$X_2]^{n+}$ ions, respectively. Such a difference reflects the different catalytic pathway followed by the reaction in the two cases. When Fe(bmen)X_2^{n+} ions are employed, the breakup of peroxide bond in the Michaelis adduct may be reasonably thought to be sterically assisted by the adjacent site in the complex, in the sense that the substrate molecule may be coordinated in a bidentate fashion.[1] Such a cyclic peroxo structure should be sterically strained so as to facilitate the cleavage of O–O bond of the bound substrate species.[1,14] On the other hand, when Fe(tetpy)X_2^{n+} ions are used, it is reasonable to assume that the diperoxy Michaelis complex decomposes through an intramolecular redox process in which the metal compound acts as an electron-transfer agent.

It is worth noting that despite the fact that the true activation energy of the reaction catalyzed by Fe(tetpy)X_2^{n+} is some 3 kcal/mol lower than that of the catalysis on Fe(bmen)X_2^{n+} ions, the rate constant for the irreversible decomposition of the Michaelis complex is only about 1.5 times higher. This implies an unfavorable entropy of activation, which in fact is found to be −32 ± 4 vs. −23 ± 5 eu, respectively (298 K). The loss of about 9 eu observed in going from the binary to the ternary adduct—which forms with Fe(bmen)X_2^{n+} and Fe(tetpy)X_2^{n+} ions, respectively—is compatible with the loss in rigidity owing to the presence of the second peroxide molecule bound to the trans derivative.[15-17] Alternatively, the difference in activation entropy between the two systems might be ascribed to different solvation phenomena which accompany the decomposition of the bimolecular and termolecular Michaelis complexes.

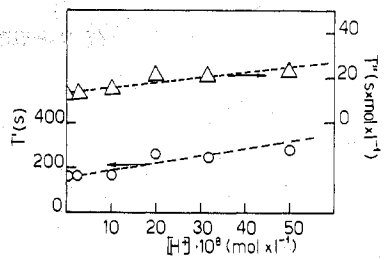

Figure 7. Dependence on $[H^+]$ of coefficients T' and T'' of the quadratic equation $y = I' + T'x + T''x^2$ of the Lineweaver–Burk curves of Figure 6 (see text).

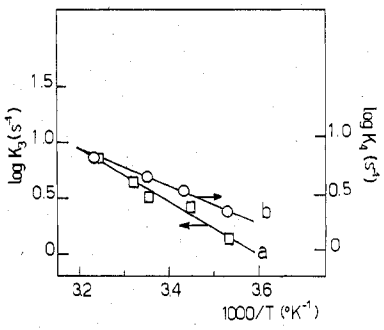

Figure 8. Arrhenius plot for the irreversible decomposition of the Michaelis "complex", which represents the rate-limiting step of the reaction catalyzed by Fe(bmen)X_2^{n+} (a) and Fe(tetpy)X_2^{n+} (b) ions; see text.

Conclusions

The overall results demonstrate that the kinetics of decomposition of hydrogen peroxide catalyzed by configurationally different iron(III) complex ions is markedly affected by the topology of the catalysts in terms of a variation in the total order of reaction as well as in the activation parameters. At high substrate concentration, an intramolecular dual active-site mechanism takes place using *trans*-Fe(tetpy)X_2^{n+} ions, which is favored by the fact that the apical sites in the complex are occupied by ligands easily displaceable by substrate molecules.[18,19] In contrast, a different active-site mechanism is observed in the case of *cis*-Fe(bmen)X_2^{n+} ions, despite the fact that the same unidentate ligands occupy the vicinal positions of the transition-metal compound. Steric hindrances are probably responsible for the lack of formation of an adduct containing two peroxide molecules coordinated in the adjacent sites of the complex.[14] The different pathway for the breakup of peroxide bond in the bound-substrate species is reflected in a different activation energy, that of the dual active-site mechanism being about 30% lower than the other one. Nevertheless, the efficiency of such a mechanism is drastically reduced by an unfavorable entropy of activation, probably due to the fact that the degrees for rotational freedom of the ternary Michaelis complex are greater than those of the binary

adduct. As a result, the turnover numbers of Fe(tetpy)X_2^{n+} and Fe(bmen)X_2^{n+} catalysts, which are 576 and 384 min^{-1}, respectively (25 °C, pH ~7.5), compare favorably with those of other metal compounds[2a,5,18] but are about 4 orders of magnitude lower than the turnover number of catalase.[20-22] Indeed, the high stability constant of the enzyme–substrate adduct[20] suggests the presence of specific binding sites in the protein surrounding the iron(III)-porphyrin prosthetic group at the active site. This could in turn imply that the substrate is held so rigidly in place to make very favorable the entropy of activation. The coupling of both factors would account for the extremely high efficiency of catalase in the decomposition of hydrogen peroxide.

Appendix

Mixed Second- and Third-Order Kinetics. If, for sake of simplicity, the $[H^+]$-independent pathways of Scheme II are only considered, eq 6 becomes

$$\frac{-d[H_2O_2]}{dt} = \frac{2k_4[C]_0[S]^2 + 2k_5[C]_0[S]K_M}{[S]^2 + [S](K_M + k_4/k_1) + K_MK_M'''} \quad (9)$$

The reciprocal form of eq 9 may be written as

$$y(x) = \frac{1 + \beta x + \beta' x^2}{\alpha + \alpha' x} \quad (10)$$

where $y = 1/V$, $x = 1/[H_2O_2]$, $\alpha = 2k_4[C]_0$, $\alpha' = 2k_5[C]_0K_M$, $\beta = (K_M + k_4/k_1)$, and $\beta' = K_MK_M'''$. Equation 10, which is formally similar to that developed for enzymatic ternary complexes formed by sequential mechanisms,[23] may be rearranged as

$$y(x) = \frac{\beta}{\alpha'} - \frac{\alpha\beta'}{\alpha'^2} + \frac{\beta'}{\alpha'}x + F(x) \quad (11)$$

where

$$F(x) = \frac{\alpha}{\alpha + \alpha' x} \frac{\alpha'^2 + \alpha^2\beta' - \alpha\alpha'\beta}{\alpha^2\alpha'^2} = \frac{\alpha}{\alpha + \alpha' x}F(0) \quad (12)$$

Since $F(x)$ decreases as x increases, it follows from (11) that for large values of x, $y(x)$ must have a linear asymptote given by

$$y_{as}(x) = \frac{\beta}{\alpha'} - \frac{\alpha\beta'}{\alpha'^2} + \frac{\beta'}{\alpha'}x \quad (13)$$

For our system this happens to be the case at $[H_2O_2]_0 < 2 \times 10^{-2}$ mol L^{-1}, as shown by the broken lines in Figure 6. Finally, from a plot of $1/(y - y_{as})$ vs. x one gets $F(0)$ and α'/α.

The method outlined above makes it possible to calculate the initial rate according to (9) or (6). For example, at pH 8 the slope of the linear portion of the curve in Figure 6 is 2.1×10^3 s and the intercept results to be -6.1×10^4 mol^{-1} L s (see eq 13). Since from the results at high $[H_2O_2]_0$ $K_M + K_M' = 0.155$ mol L^{-1} and $k_4 = 4.8$ s^{-1}, then $k_5K_M = 0.153$ mol L^{-1} s^{-1} and $K_MK_M''' = 6.4 \times 10^{-2}$ mol^2 L^{-2} (25 °C). With these parameters, the velocity calculated according to eq 9 is $V_0 = 2.1 \times 10^{-6}$ mol L^{-1} s^{-1} ($[C]_0 = 1 \times 10^{-4}$, $[H_2O_2]_0 = 4 \times 10^{-3}$ mol L^{-1}, 25 °C). Despite the crudeness of the calculation procedure, owing to the fact that the data at low substrate concentration are few, this value agrees rather satisfactorily with that experimentally determined (1.73×10^{-6} mol L^{-1} s^{-1}).

Registry No. H_2O_2, 7722-84-1; *cis*-Fe(bmen)$(OH)_2^+$, 62905-74-2; *trans*-Fe(tetpy)$(OH)_2^+$, 61412-01-9.

References and Notes

(1) J. H. Wang, *J. Am. Chem. Soc.*, **77**, 822, 4715 (1955); R. C. Jarning and J. H. Wang, *ibid.*, **80**, 786 (1958); J. H. Wang, *Acc. Chem. Res.*, **3**, 90 (1970).
(2) (a) M. L. Kremer, *Nature (London)*, **205**, 384 (1965); (b) M. L. Kremer, *Trans. Faraday Soc.*, **61**, 1453 (1965); R. Gatt and M. L. Kremer, *ibid.*, **64**, 721 (1968).
(3) S. B. Brown and P. Jones, *Trans. Faraday Soc.*, **64**, 994, 999 (1968).
(4) G. A. Hamilton, *Adv. Enzymol.*, **32**, 55 (1969).
(5) P. Waldmeier and H. Sigel, *Inorg. Chim. Acta*, **5**, 659 (1971).
(6) M. Branca, P. Checconi, and B. Pispisa, *J. Chem. Soc., Dalton Trans.*, 481 (1976).
(7) M. Branca, B. Pispisa, and C. Aurisicchio, *J. Chem. Soc., Dalton Trans.*, 1543 (1976).
(8) M. Cerdonio, F. Mogno, B. Pispisa, G. L. Romani, and S. Vitale, *Inorg. Chem.*, **16**, 400 (1977).
(9) H. Lineweaver and D. Burk, *J. Am. Chem. Soc.*, **56**, 658 (1934).
(10) D. Margerison in "Comprehensive Chemical Kinetics", Vol. 1, C. H. Bamford and C. F. H. Tipper, Eds., Elsevier, Amsterdam, 1969, Chapter 5.
(11) M. Barteri and B. Pispisa, *Gazz. Chim. Ital.*, **106**, 499 (1976).
(12) See, for example, F. C. Neuhaus, *J. Biol. Chem.*, **237**, 3128 (1962).
(13) M. Barteri, M. Farinella, B. Pispisa, and L. Splendorini, *J. Chem. Soc., Faraday Trans. 1*, **74**, 288 (1978).
(14) M. Barteri, M. Farinella, and B. Pispisa, *Biopolymers*, **16**, 2569 (1977).
(15) M. L. Bender, F. J. Kezdy, and C. R. Gunter, *J. Am. Chem. Soc.*, **86**, 3714 (1964).
(16) H. A. Scheraga, "Protein Structure", Academic Press, New York, N.Y., 1961, p 40.
(17) P. D. Barlett and R. R. Hiatt, *J. Am. Chem. Soc.*, **80**, 1402 (1958).
(18) H. Sigel, B. Prijs, P. Rapp, and F. Dinglinger, *J. Inorg. Nucl. Chem.*, **39**, 179 (1977).
(19) M. Barteri, M. Farinella, and B. Pispisa, *J. Inorg. Nucl. Chem.*, **40**, 1277 (1978).
(20) P. Jones and W. F. K. Wynne-Jones, *Trans. Faraday Soc.*, **58**, 1148 (1962), and references cited therein.
(21) P. Jones and A. Suggett, *Biochem. J.*, **110**, 617 (1968).
(22) M. L. Kremer and S. Baer, *J. Phys. Chem.*, **78**, 1919 (1974); E. Zidoni and M. L. Kremer, *Arch. Biochem. Biophys.*, **161**, 658 (1974).
(23) G. Pettersson, *Acta Chem. Scand.*, **23**, 2717 (1969); "Structure and Function of Oxidation-Reduction Enzymes", Å. Åkeson and A. Ehrenberg, Eds., Pergamon Press, Oxford, 1972, p 739.